

Flaw Tolerance and Toughness Curves in Two-Phase Particulate Composites: SiC/Glass System

Hongda Cai,* Nitin P. Padture,* Bryan M. Hooks** & Brian R. Lawn

Materials Science and Engineering Laboratory, National Institute of Standards and Technology, Gaithersburg, Maryland 20899, USA

(Received 11 March 1993; accepted 10 September 1993)

Abstract

Flaw-tolerance and associated toughness-curve (T-curve) characteristics in SiC/glass particle/matrix composites are studied. Two glass compositions, chosen to produce composites at extremes of high (H) and low (L) thermal expansion mismatch relative to the SiC particles, are investigated. In-situ observations of crack extension from indentation flaws reveal widely different responses: in the L composite the path is relatively undistorted from the planar geometry, with trans-particle fractures; in the H composite the path deflects strongly around the particles, with consequent interfacial bridge formation and activity in the crack wake. Surface fracture patterns produced by spherical indenters confirm the implied transition from trans-particle to inter-particle fracture with increasing internal residual stress, and point to a potential degradation in short-crack properties like wear and fatigue. Indentation–strength measurements also show different characteristics in the two composites: minor flaw tolerance in the L material, consistent with a single-valued, ‘rule of mixtures’ toughness; major tolerance in the H material, consistent with a pronounced T-curve. The T-curves themselves are deconvoluted from the indentation–strength data for each composite and analyzed.

Fehlertoleranz und damit verbundene Charakteristika der Rißwiderstandskurven (R-Kurven) von SiC/Glas (Teilchen/Matrix) Verbundwerkstoffen wurden untersucht. Zwei Glaszusammensetzungen, die so gewählt wurden, daß der thermische Ausdehnungskoeffizient entweder extrem groß (H) oder klein (L) im Vergleich zu dem der SiC-Teilchen war, wurden

untersucht. In-situ Beobachtung der Rißausbreitung ausgehend von Defekten verursacht durch Eindrücke zeigen stark unterschiedliche Verhaltensweisen: in den L-Verbundwerkstoffen weicht der Rißpfad relativ wenig von ebener Geometrie ab, die Risse verlaufen transgranular; in dem H-Verbundwerkstoff wird der Rißpfad um die Teilchen herumgelenkt, was zur Folge hat, daß zwischen den Grenzflächen Brücken gebildet werden und Wechselwirkungen zwischen den Rißflanken entstehen. Oberflächenbruchspiegel, die durch Kugeleindrücke erzeugt wurden, bestätigen den Übergang von transgranularem zu intergranularem Rißwachstum bei zunehmenden inneren Spannungen und weisen auf eine mögliche Verschlechterung der Verschleiß- und Ermüdungseigenschaften hin. Festigkeitsmessungen an mit Härteeindrücken versehenen Proben zeigen ebenfalls unterschiedliche Eigenschaften der beiden Verbundwerkstoffe: geringere Fehlertoleranz im L-Material, konsistent mit der ‘Mischungsregel’; größere Toleranz im H-Material, konsistent mit einer ausgeprägten R-Kurve. Die R-Kurven werden aus den Härteeindruck–Festigkeit-Daten für jeden Verbundwerkstoff analysiert.

On étudie la tolérance aux défauts et les caractéristiques associées de la courbe de ténacité dans des composites de verre à particules de SiC. On s'intéresse à deux compositions de verres, choisis afin d'obtenir des désaccords dus à l'expansion thermique extrême, l'un élevé (H), l'autre faible (L). L'observation in situ de l'extension des fissures à partir de marques d'indentation révèle des comportements très différents: dans le composite L, la trajectoire de la fissure est pratiquement plane, avec fracture transgranulaire des particules; dans le composite H, la trajectoire est fortement défléchie autour des particules, et il y a donc formation de ponts de liaison aux interfaces ainsi que de l'activité dans le sillon de la fissure. Les motifs des surfaces de fractures produits par des indentateurs sphériques confirment qu'il y a transition d'un mode de

* Guest Scientist from: Department of Materials Science and Engineering, Lehigh University, Bethlehem, PA 18015, USA.

** Present address: Harvard University, Cambridge, MA 02138, USA.

fracture transparticulaire à un mode interparticulaire lorsque la contrainte résiduelle interne augmente, et montre qu'il peut alors y avoir dégradation des propriétés du matériau liées aux fissures courtes, comme le comportement à l'usure ou en fatigue. Les expériences d'indentation et de résistance présentent des caractéristiques différentes pour les deux composites: une tolérance faible aux défauts dans le matériau L, cohérente avec une valeur unique de la ténacité qui suit une 'loi des mélanges', une tolérance élevée dans le matériaux H, correspondant à une courbe de ténacité prononcée. Les courbes de ténacité elles-mêmes ont été déconvoluées à partir des données d'indentation et de tests de résistance, et analysées.

1 Introduction

It is now well established that the existence of crack-size-dependent toughness functions, i.e. toughness curves (T -curves, or R -curves), in non-transforming monophase ceramics is primarily attributable to grain bridging in the crack wake.^{1–12} An important manifestation of T -curve behavior is 'flaw tolerance', i.e. a relative insensitivity of strength to initial flaw size.^{11,13,14} Designers of high reliability ceramic materials with superior long-crack toughness seek to optimize such flaw-tolerance characteristics.

More recently, this connection of the T -curve and its associated flaw tolerance with crack bridging has been shown to extend to particle-reinforced ceramics.^{15,16} Fracture mechanics modeling of bridging in two-phase ceramics identifies the T -curve with key microstructural variables like volume fraction, particle size and residual thermal expansion mismatch stress.^{17,18} To date, $\text{Al}_2\text{TiO}_5/\text{Al}_2\text{O}_3$ has been the material system of choice for analysis, because of the strong T -curve enhancement associated with its inordinately high mismatch stresses. However, those same high residual stresses impose severe limits on the capacity of the experimentalist to investigate the role of microstructural variables:¹⁸ the material undergoes bulk microcracking at relatively small volume fraction and particle size, and the residual stress itself for this system is not subject to variation.

In the present paper these limitations are rectified by studying the T -curve and flaw-tolerance characteristics of model two-phase particulate ceramic composites of SiC particles in a compositionally variable silicate glass matrix. A major advantage of the proposed SiC/glass system, apart from ease of fabrication, is the facility to control and vary the microstructural parameters. In particular, the internal residual stress can be prescribed by adjusting the glass matrix composition. In-situ microscopic observations of crack extension from indentation flaws are used to provide direct evidence of

inter-particle fracture and ensuing bridge formation as a dominant fracture mode in a SiC/glass composite with high internal stresses. By contrast, similar observations in a composite with *low* internal stresses reveal primarily trans-particle fracture, with comparatively little bridging. Hertzian indentation tests confirm this difference in fracture mode, with implications concerning prospective wear and fatigue properties. Indentation–strength tests confirm the predicted correlation between flaw tolerance and internal stress, and enable determinations of the underlying T -curves.

The use of model two-phase ceramic/matrix systems in the study of brittle fracture is not new. Compelling evidence for strength and toughness enhancements from incorporation of second-phase particles has been presented in several earlier studies.^{19–26} However, little effort was made in those earlier studies to consider the enhancements in relation to a systematically varying toughness curve. Nor was any direct (in-situ) identification made of the responsible agents of crack inhibition; thus, whereas crack deflection, crack pinning and bowing, and frontal-wake zone microcracking have been variously proposed as toughening mechanisms, crack–interface bridging has, until recently, passed unnoticed.

2 Experimental Procedure

2.1 Materials

Composites of SiC particles in silica glass matrices were fabricated for fracture studies. Two glass compositions with different thermal expansion mismatch relative to SiC were chosen to provide high (H) and low (L) levels of compression stress in the SiC particles, Table 1. Glass L, an alkaline-earth aluminosilicate, was obtained commercially as slabs (Glass Code 1723, Corning Inc., Corning, NY). Glass H, a sodium–magnesium silicate, was prepared in the authors' laboratories from reagent-grade raw materials (60% SiO_2 , 25% Na_2O , 15% MgO , Fisher Scientific, Fair Lawn, NJ), as described in the following paragraphs. The SiC particles were obtained commercially as abrasive grit, mean diameter $30\ \mu\text{m}$ (37 Crystolon, Norton Company, Worcester, MA).

With glass H, a 300 g batch of blended powder was dry-blended and melted in a platinum crucible at 1500°C for 2 h. The melt was continuously stirred with a platinum rod to ensure homogeneity. One portion of the melt was quenched in water. The remaining portion was cast into a slab and annealed at 500°C for 1 h, followed by slow cooling.

The quenched portion of glass H and as-received slabs of glass L were separately pulverized in a

Table 1. Constituent properties of the SiC-particle/glass-matrix composites

	Expansion coefficient α ($10^{-6} \text{ } ^\circ\text{C}^{-1}$)	Young's modulus E (MPa)	Hardness H (GPa)	Cooling temperature ΔT ($^\circ\text{C}$)	Residual stress ^a σ_R (MPa)	Toughness T_0 ($\text{MPa m}^{1/2}$)
SiC	4.5 ^b	436	24	—	—	4.0 ^e
Glass H	12.7 ^c	63	5.0	419	308	0.75 ^f
Glass L	4.6 ^d	90	6.0	685	8	0.91 ^f

^a Computed from $\sigma_R = (\alpha_0 - \alpha_p)\Delta T / [(1 + \nu_0)/2E_0 + (1 - 2\nu_p)/E_p]$ for particle P in matrix 0.²⁷

^b Ref. 28.

^c Ref. 29.

^d Corning Glass works, Material Information, 1984.

^e Refs 30 and 31.

^f Ref. 32.

zirconia ring mill and sieved (No. 320 mesh). Each glass was mixed with 20 vol.% SiC particles in methanol and Teflon media in polyethylene bottles. The mixtures were then blended in a ball mill for 24 h to form consistent slurries. These were poured into Teflon beakers and dried while continuously stirring on a hot plate. The resulting powders were calcined at 375°C for 24 h. A 60 g batch of each powder composition was rolled in a plastic bag to break up any agglomerates, before transferring to a graphite die. Hot pressing was then carried out in a vacuum hot press (Vacuum Industries, Nashua, NH) at a pressure 10 MPa for 30 min, at temperatures 650°C for composite H and 980°C for composite L, to form disks 75 mm diameter by 6 mm thickness. The hot-pressing temperatures were chosen to correspond to a viscosity of 0.1 MPa s, somewhat higher than the softening points of glasses H²⁹ and L (Corning Glass Works, Material Information, 1984). The disks were cooled to 50°C above the annealing point at a cooling rate of 10°C min⁻¹, and subsequently to room temperature at 2°C min⁻¹.

Flexure bar specimens 25 × 4 × 4 mm were cut from the hot-pressed composites and the base glass slabs for indentation-strength tests. The specimen edges were chamfered (10 μm diamond grinding wheel) and polished (6 μm diamond paste), to minimize edge failures. The prospective tensile faces of all specimens were given a final polish to 1 μm.

Some polished specimens were etched in 5% hydrofluoric acid solution to check for the presence of microcracks.

2.2 Hertzian indentation tests

Simple Hertzian tests were made on some of the polished surfaces of the high-internal-stress (H) and low-internal-stress (L) SiC/glass composites, as well as on the base glasses as controls. The indenters were made with tungsten carbide spheres, radius 1.98 mm, load 500 N. All tests were carried out in laboratory air, relative humidity 40–50%, under which conditions moisture may assist in fracture initiation.³³

The presence of surface cracking at the indentation sites was revealed by coating the contacted surfaces with gold and viewing in Nomarski interference contrast.

2.3 In-situ tests

Selected specimens of each of the H and L SiC/glass composites were indented at their polished-face centers with a Vickers diamond pyramid, at fixed load 100 N, with the radial crack arms aligned parallel and perpendicular to the bar edges. Each indentation site was covered with a drop of dry silicone oil, to minimize subsequent moisture-assisted slow crack growth, plus a glass cover slip, to facilitate clear observation of the surface cracks.

A loading fixture mounted onto the stage of an optical microscope was used for in-situ observations of radial crack responses in four-point flexure.³⁴ The indented specimens were loaded slowly using a piezoelectric driver, and the ensuing crack growth relative to the particulate composite microstructure monitored on a videocassette recorder and intermittently photographed.

2.4 Indentation-strength tests

Each remaining flexure specimen was Vickers indented at its polished-face center, at a prescribed load within the range 3 to 300 N. Care was again taken to align the radial cracks along the specimen edges. All indentations were made in the laboratory ambient, allowed to stand for 5 min, and then covered with a drop of dry silicone oil to minimize environmental effects in the ensuing strength tests.

The indented specimens were tested in a four-point bend fixture (outer span 20 mm, inner span 10 mm) mounted on a universal testing machine (Model 1122, Instron Corp., Canton, MA). The fracture times were kept below 50 ms, to ensure near 'inert' testing conditions. Failed specimens were examined in an optical microscope to confirm that the failures originated from the indentations. Specimens that failed from the other sources were

included in the data pool for unindented specimens.^{13,30}

3 Qualitative results

3.1 Hertzian tests

Micrographs of Hertzian indentations on L and H SiC/glass surfaces are shown in Fig. 1. The damage in the low-internal-stress composite L, Fig. 1(A), is typical of the classical Hertzian cone fracture,³⁵⁻³⁷ i.e. near-circular surface traces. These traces do not deviate substantially from those observed in control tests on the base L glass itself (not shown here), indicating that the crack paths within the radial tensile stress field around the contact circle^{35,36} are relatively undistorted by the SiC particulate phase. The pattern is indicative of a material with trans-particle fracture characteristics.

The damage in the high-internal-stress composite H, Fig. 1(B), shows a very different response. The

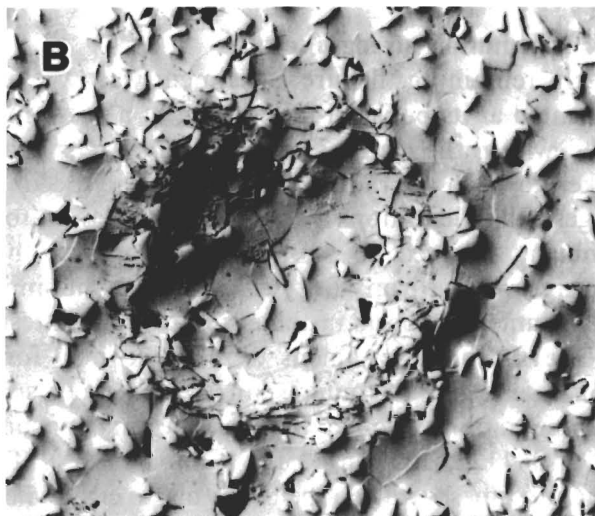
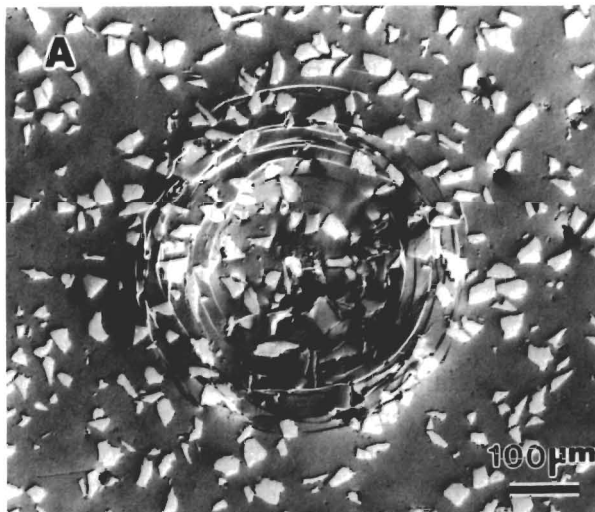


Fig. 1. Damage patterns in SiC/glass, (A) low-internal-stress (L) and (B) high-internal-stress (H), composites. Tests made with tungsten carbide sphere of radius 1.98 mm at load 500 N, in laboratory ambient conditions.

Hertzian fracture is comparatively ill-defined, consisting more of linked-up particle-initiated microcracks than regular circular macrocracks. These microcracks are not oriented normally to the contact radial direction in the manner of classical Hertzian fractures, indicating that the crack driving forces are now dominated by the residual internal tensile stresses.³⁸ In this case the damage may be more properly characterized in terms of *inter-particle* fracture. Note that individual microcracks extend only over a few inter-particle dimensions, implying that the superimposed microstructural field contains compressive stresses as well as tensile. The interplay between tensile and compressive internal stresses is an important ingredient of grain- or particle-interlock bridging.¹¹

3.2 In-situ observations of Vickers cracks

Optical micrographs of the wake regions of cracks grown from Vickers indentations under applied flexure stresses in the low-internal stress (L) and high-internal-stress (H) composites are shown in Fig. 2. The ultimate stress levels correspond to $\approx 70\%$ of the strength in both cases.

In composite L, Fig. 2(A), the cracks follow more or less straight, classical radial trajectories. In-situ observations of the crack evolution up to this point revealed intermittent interruption of the extension by the SiC particles. When such interruption did occur, further increase in the applied load was necessary to force the crack through the arresting particle. At such points the crack 'popped in', occasionally propagating through the next two or three particles in the immediate path. Once broken, the obstructing grains rarely appeared to provide any further resistance to the extension; i.e. bridges were not formed, except perhaps when the advancing crack intersected the particle/matrix interface at an unusually oblique angle of incidence. On further stressing beyond the configuration in Fig. 2(A) the crack grew to failure along essentially the same crack plane.

By contrast, the fracture in composite H, Fig. 2(B), shows an entirely different behavior. The cracks often emerge away from the indentation corners and trace a much more disruptive path, again suggestive of a dominant role by local residual stresses. In-situ observations revealed a highly erratic evolution at the microscopic level in this material. Under increasing applied stress the crack popped in from particle to particle, deviating markedly from segment to segment, yet all the while remaining highly stable at the macroscopic level. At some points the crack reinitiated abruptly on the far side of an arresting particle. At others an isolated microcrack appeared to form at a particle some distance ahead of the primary crack tip, with abrupt coalescence at

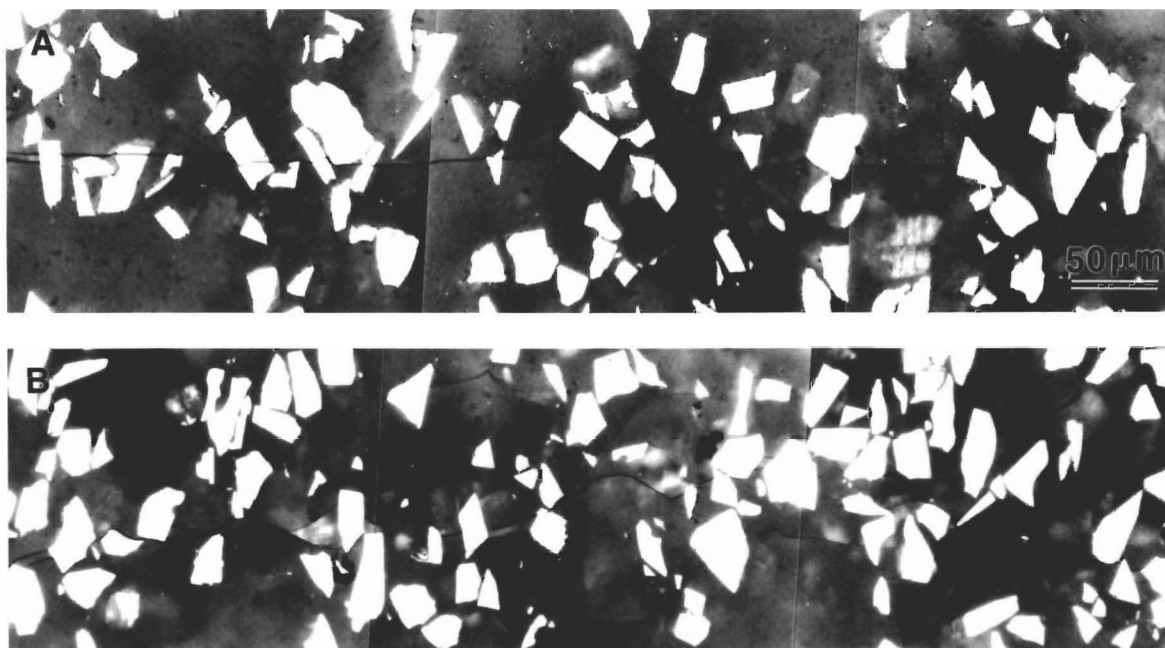


Fig. 2. In-situ optical micrographs of Vickers radial cracks in SiC composites under flexure stress, (A) composite L, (B) composite H. Indentation impression formed at load 100 N, outside field of view at left.

some increment in the load. Notwithstanding the fact that previous investigations in alumina ceramics² suggest that such apparently isolated microcracks may well be pre-connected to the primary crack in the subsurface, such geometrical deflections are especially conducive to the formation of particulate bridges at the crack interface. The in-situ observations confirmed the existence of several persistently active bridge sites in Fig. 2(B), up to distances ≈ 1 mm behind the crack tip.

On further stressing, the crack in Fig. 2(B) continued its erratic growth until, ultimately, it spanned almost the entire specimen width. During these final loading stages microcracks began to pop in over the entire surface of the glass matrix. Similar applied-stress-induced microcracking has been reported in the $\text{Al}_2\text{TiO}_5/\text{Al}_2\text{O}_3$ system.³⁹ Such observations indicate that composite H is close to the limit for spontaneous microcracking. In fact, stress-free specimens left lying in the laboratory ambient conditions for periods of several weeks gradually developed extensive networks, as seen in the etched surface of Fig. 3. On the other hand, no distinctive frontal-wake microcrack cloud was observed at any stage of the crack propagation in the experiments.

3.3 Indentation–strength

Strength–indentation load data for the low-internal-stress (L) and high-internal-stress (H) systems are plotted in Figs 4 and 5, respectively. Each data point with error bar is the mean and standard deviation of 4 to 6 specimens. In these diagrams the upper data set represents the composite, the lower data set the

base glass. The hatched regions at left represent breaks from other failure sources, edge flaws in the base glasses and SiC particles in the composites.

It is immediately clear that, within the given indentation load range, the addition of SiC particles substantially improves the stress-bearing capacity of the materials. Both base glasses show a classical flaw sensitivity in the strength characteristics ($P^{-1/3}$ load dependence—Section 4). In composite H, the improvement is manifested primarily as an enhanced flaw tolerance, with a modest ‘plateau’ strength. In composite L, the improvement is more in the form of a uniformly enhanced strength over the indentation load (indentation flaw size) range, with minimal development of flaw tolerance. Therefore,

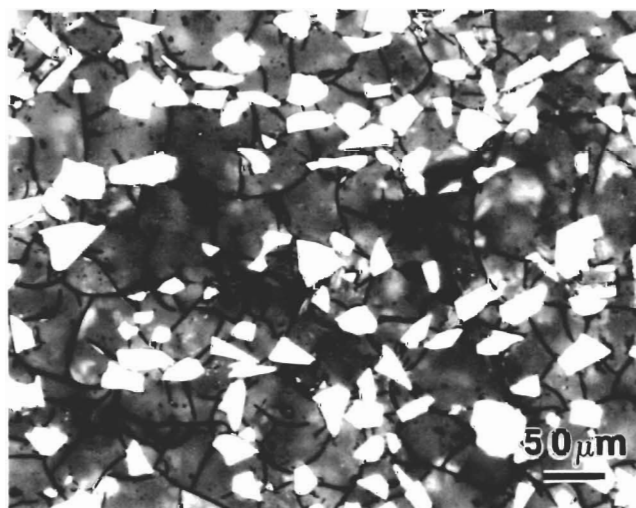


Fig. 3. Etched surface of SiC glass composite H, after prolonged exposure (4 weeks) to laboratory ambient conditions. Note moisture-enhanced development of microcrack network.

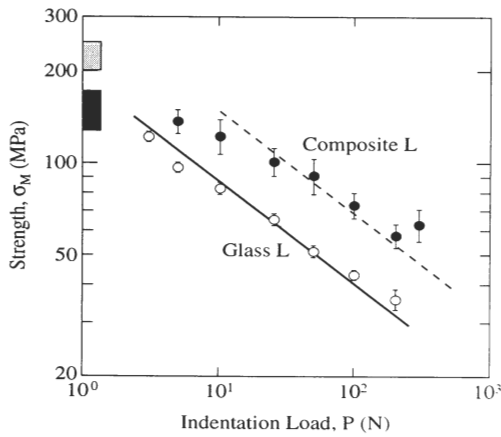


Fig. 4. Indentation–strength data for glass L and corresponding SiC/glass composite L. Each datum point represents mean and standard deviation of strengths from 4 to 6 specimens. The light and dark shaded areas at left represent strengths of unindented specimens for the glass and the composite, respectively. Solid line through glass data is fit to eqn (3) using single-valued toughness for glass L. Dashed line is prediction for SiC/glass composite L, using single-valued toughness from rule of mixtures.

extrapolating beyond the data range, it may be concluded that composite H demonstrates superior toughness properties at high indentation loads (long-crack region), but inferior toughness properties at low indentation loads (short-crack region).

4 Quantitative Evaluation of T -Curves

Now the T -curve function $T(c)$, with c the crack size, is deconvoluted from the indentation–strength data.³⁴ At equilibrium, the ‘global’ K -field for a radial crack system formed at contact load P and

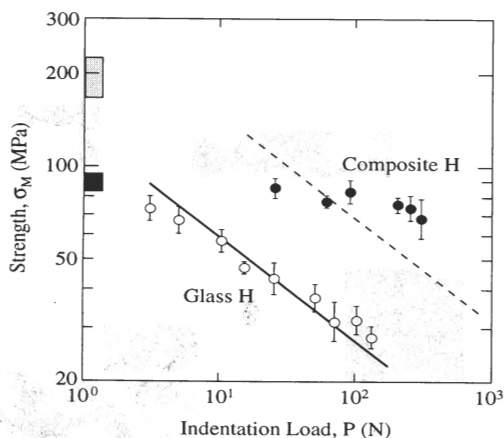


Fig. 5. Indentation–strength data for glass H and corresponding SiC/glass composite H. Each datum point represents mean and standard deviation of strengths from 4 to 6 specimens. The light and dark shaded areas at left represent strengths of unindented specimens for the glass and the composite, respectively. Solid line through glass data is fit to eqn (3) using single-valued toughness for glass H. Dashed line is prediction for SiC/glass composite H, using single-valued toughness from rule of mixtures.

subjected to subsequent applied stress σ_A can be expressed as

$$K'_A(c) = K_A(c) + K_R(c) = \psi\sigma_A c^{1/2} + \chi P/c^{3/2} = T(c) \quad (1)$$

where ψ is a crack geometry coefficient and χ is a residual-contact-field coefficient. For a given P , failure occurs at that value of applied stress $\sigma_A = \sigma_M$ that satisfies the ‘tangency conditions’⁴⁰

$$dK'_A(c)/dc = dT(c)/dc \quad (2)$$

It follows that the T -curves for the composites can be determined as the envelopes to the families of $K'_A(c)$ curves constructed from the (σ_M, P) data sets in Figs 4 and 5.³⁴

In order to construct such $K'_A(c)$ curves, it is necessary first to ‘calibrate’ the coefficients ψ and χ in eqn (1) for the matrix glasses. The key to a simplified calibration is the single-valuedness of the matrix toughness, $T = T_0$ for these homogeneous materials.³⁴ Inserting $T = T_0$ into eqns (1) and (2) then yields the familiar analytical strength–load relation^{37,41}

$$\sigma_M = (3T_0/4\psi)(T_0/4\chi P)^{1/3} \quad (3)$$

Hence values for the compound parameter $T_0^4/\psi\chi^{1/3}$ may be obtained from best fits to the data for the base glasses in Figs 4 and 5. It is assumed here that ψ is a material-independent crack geometry coefficient, and the value $\psi = 0.77$ obtained previously from data on a fine-grain alumina is retained.³⁴ Then, using the T_0 values from Table 1, $\chi = 0.024$ for glass L and $\chi = 0.035$ for glass H are obtained.

Next consider the effect of adding the SiC phase. It has already been intimated that the geometrical coefficient ψ is not sensitive to material variations. The coefficient χ , on the other hand, varies with $(E/H)^{1/2}$, where E is Young’s modulus and H is the hardness.⁴² Using the rules of mixtures for a ‘Voigt’ two-phase particle/matrix ($P/0$) composite (C) with volume fractions $V_0 + V_P = 1$,

$$E_C = V_0 E_0 + V_P E_P \quad (4a)$$

$$H_C = V_0 H_0 + V_P H_P \quad (4b)$$

it may be verified from Table I that the changes in E/H from addition of 20 vol.% SiC amount to less than 10% for each glass. To a first approximation, therefore, the coefficients ψ and χ may be considered essentially unchanged by addition of the second phase.

Families of $K'_A(c)$ curves for the L and H SiC/glass composites are plotted in Figs 6 and 7 using the (σ_M, P) data from Figs 4 and 5. The fitted T -curves are envelopes of tangency points to these families of curves. The lower dashed lines are toughness values T_0 for the base glasses. The upper dashed lines are ‘rule-of-mixtures’ toughness values T_C for the

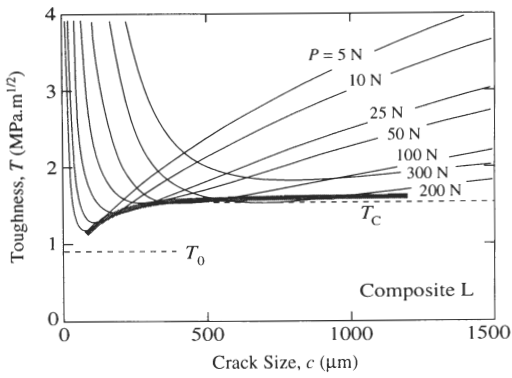


Fig. 6. T -curve construction for SiC/glass composite L. Solid curves are plots of global K -field function $K'_A(c)$ in eqn (3), evaluated for each strength $\sigma_A = \sigma_M$ and load P in Fig. 4. Shaded band is an empirically fitted T -curve envelope.³⁴ Lower horizontal dashed line is toughness T_0 for base glass; upper horizontal dashed line is rule-of-mixtures toughness T_C for the composite.

composites, evaluated for an ideal planar crack intersecting the second-phase particles in the absence of bridging or other extraneous energy absorbing process; these values are calculable from Table 1 by writing an expression for the reversible work to separate unit area of crack plane,

$$R_C = V_0 R_0 + V_P R_P \quad (5)$$

and invoking the familiar plane stress relation $R = T^2/E$ ³⁷ along with eqn (4a) to obtain

$$T_C = [V_0(E_C/E_0)T_0^2 + V_P(E_C/E_P)T_P^2]^{1/2} \quad (6)$$

For the low-internal-stress composite L in Fig. 6 the shaded T -curve envelope is fitted empirically to the $K'_A(c)$ curves.³⁴ This fitted curve virtually overlaps the $T = T_C$ line at $c > 200 \mu\text{m}$, and deviates slightly below T_C at $c < 200 \mu\text{m}$. Thus the toughness behavior of the L composite is consistent with a predominantly trans-particle mode of fracture (Figs 1(A) and 2(A)).

The response is markedly different for the *high-*

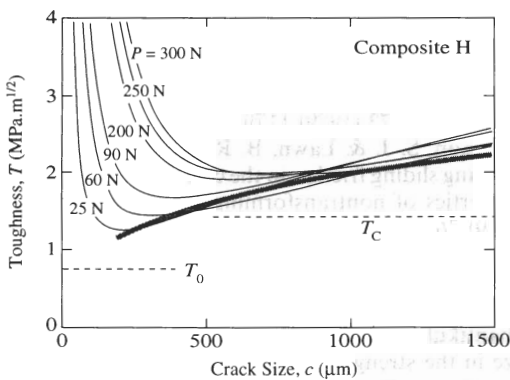


Fig. 7. T -curve construction for SiC/glass composite H. Solid curves are plots of global K -field function $K'_A(c)$ in eqn (3), evaluated for each strength $\sigma_A = \sigma_M$ and load P in Fig. 5. Shaded curve is fitted T -curve from the bridging model, eqn (7). Lower horizontal dashed line is toughness T_0 for base glass; upper horizontal dashed line is rule-of-mixtures toughness T_C for the composite.

internal-stress composite H in Fig. 7. In this case the T -curve crosses the $T = T_C$ line at $c \approx 400 \mu\text{m}$, and extends well above this line in the long-crack region. This highly enhanced long-crack toughness is consistent with a predominantly inter-particle (Fig. 1(B)), strong-bridging (Fig. 2(B)) mode of fracture. Accordingly, the T -curve in Fig. 7 has been plotted using an analytical expression for $T(c)$ derived for the simple bridging model in Fig. 8:^{17,18}

$$T(c) = T_0 - \psi qc^{1/2} \quad (0 \leq c \leq \lambda) \quad (7a)$$

$$T(c) = T_0 + \psi pc^{1/2} \times \{1 - [1 - (1 - \lambda/c)^2]^{1/2}\} - \psi qc^{1/2} [1 - (1 - \lambda/c^2)]^{1/2} \quad (\lambda \leq c \leq \Lambda + \lambda) \quad (7b)$$

$$T(c) = T_0 + \psi pc^{1/2} \times \{[1 - (1 - \Lambda/c - \lambda/c)^2]^{1/2} - [1 - (1 - \lambda/c^2)]^{1/2} - \psi qc^{1/2} [1 - (1 - \lambda/c)^2]^{1/2} \quad (\Lambda + \lambda \leq c) \quad (7c)$$

where p and q are averaged long-crack closing and short-crack opening stresses from the matrix/particle mismatch acting over characteristic bridging zone dimensions λ and Λ ; the fit corresponds to parameter adjustments $p = 66 \text{ MPa}$, $(p + q)(2\lambda)^{1/2} = 0.40 \text{ MPa m}^{1/2}$ and $\Lambda = 840 \mu\text{m}$.¹⁷

It is noteworthy that the bridging model of Fig. 8, with its assumption of a crack always constrained to the matrix (implicit by the appearance of T_0 rather than T_C as the base toughness in eqn (7)), could not be made to provide a satisfactory fit to the L composite data in Fig. 6.

5 Discussion

The present study has demonstrated that thermal expansion mismatch can have a dominant influence in the toughness and strength properties of two-phase ceramics, first by controlling the genesis and second by controlling the effectiveness of crack/interface bridging. As shown in the micro-

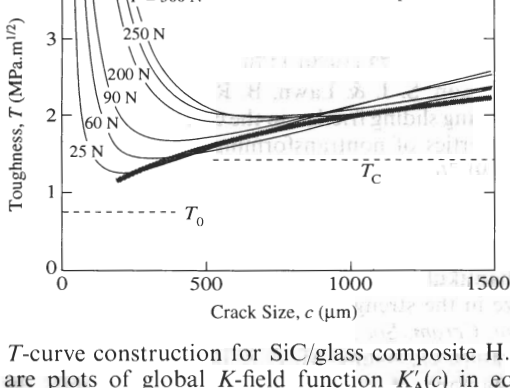


Fig. 8. Model of bridged crack.¹⁷ Compressed particles exert opening stress on matrix in near-tip crack-plane region, closure (bridging) stresses beyond.

graphs of cracks in SiC/glass composites in Figs 1 and 2, increasing the residual stress from low level (composite L) to high level (composite H) results in a transition from predominantly trans-particle to predominantly inter-particle fracture. Inter-particle fracture is promoted by an increase in stress-directed crack deflection, which enhances bridge formation, and in particle/matrix pullout friction, which inhibits bridge rupture.^{17,18} The end result is an enhanced *T*-curve for the H composite, Fig. 7, relative to the L composite, Fig. 6.

This *T*-curve enhancement from bridging in two-phase composites is manifested most compellingly in the indentation–strength characteristics of Figs 4 and 5. Composite L in Fig. 4 shows relatively little flaw tolerance, consistent with a single-valued, rule-of-mixtures toughness. Composite H in Fig. 5 shows substantially greater flaw tolerance, with strengths higher than the simple rule-of-mixtures prediction over most of the load range covered. On the other hand, extrapolation of the composite H strength data into the low-load region implies a depressed *T*-curve, with the suggestion of diminished short-crack properties. Hence while increased internal-stress-enhanced bridging results in higher long-crack toughness, tensile components of the same internal-stress field conversely lead to lower practical strength. These same tensile stresses also greatly increase the susceptibility to local microfracture, as in Fig. 1(B), and thence to brittle wear³⁸ and fatigue.⁴³ A long-crack/short-crack tradeoff is in effect here. One might attempt to explain any such tradeoff from incorporation of a second phase in terms of a traditional ‘critical flaw’ argument: short-crack strength is decreased by introducing larger flaws; long-crack toughness is increased by providing geometrical ‘obstacles’ to crack propagation, e.g. by crack deflection, crack pinning and bowing (Section 1). However, the simple ‘obstacle’ concept can not account for the improvement in flaw tolerance with increase in thermal mismatch—it contains no provision for a cumulative *T*-curve.³⁷ In this context it may be recalled that no evidence for the existence of a detached microcrack cloud, which might alternatively account for the *T*-curve, was found in the H composite.

The last point pertaining to microcracking warrants comment in the context of microstructural design. It is clear from the present study that one may control the toughness and strength properties, and even the mode of crack propagation, by tailoring the composite microstructure. In particular, increasing the thermal mismatch between particles and matrix (as well as particle size and volume fraction^{17,18}) enhances the bridging long-crack toughness, and hence the flaw tolerance. However, beyond a certain limit this increase in thermal mismatch (or particle

size or volume fraction) generates critical local tensile fields, initiating bulk microcracking and, ultimately, degrading the strength.⁴⁴ It is clear from Fig. 3 that the materials processor who seeks to optimize microstructures for long-crack toughness should pay due attention to such limits, with additional allowance for the deleterious time-dependent effects of moisture.

Acknowledgements

The authors thank Prabhat Gupta for useful advice on the glass compositions, Dale Kauffman for assistance with the glass melting procedures, and Linda Braun for assistance with the in-situ experiments. Funding for this work was provided by the US Air Force Office of Scientific Research.

References

1. Knehans, R. & Steinbrech, R., Memory effect of crack resistance during slow crack growth in notched Al₂O₃ bend specimens. *J. Mater. Sci. Lett.*, **1** (1982) 327–9.
2. Swanson, P. L., Fairbanks, C. J., Lawn, B. R., Mai, Y.-W. & Hockey, B. J., Crack–interface grain bridging as a fracture resistance mechanism in ceramics: I. Experimental study on alumina. *J. Am. Ceram. Soc.*, **70** (1987) 279–89.
3. Mai, Y.-W. & Lawn, B. R., Crack–interface grain bridging as a fracture resistance mechanism in ceramics: II. Theoretical fracture mechanics model. *J. Am. Ceram. Soc.*, **70** (1987) 289–94.
4. Steinbrech, R. W., Reichl, A., Deuerler, F. & Schaarwachter, W., Correlation of crack opening displacement and crack resistance curve of alumina. *Sci. Ceram.*, **14** (1987) 659–64.
5. Swanson, P. L., Crack–interface traction: A fracture-resistance mechanism in brittle polycrystals. In *Fractography of Glasses and Ceramics*, Vol. 22, American Ceramic Society, Columbus, OH, 1988, pp. 135–55.
6. Reichl, A. & Steinbrech, R. W., Determination of crack bridging forces in alumina. *J. Am. Ceram. Soc.*, **71** (1988) C299–C301.
7. Sakai, M., Yoshimura, J., Goto, Y. & Inagaki, M., *R*-Curve behavior of a polygranular graphite; microcracking and grain bridging in the wake region. *J. Am. Ceram. Soc.*, **71** (1988) 609–16.
8. Beauchamp, E. K. & Monroe, S. L., Effect of crack–interface bridging on subcritical crack growth in ferrites. *J. Am. Ceram. Soc.*, **72** (1989) 1179–84.
9. Bennison, S. J. & Lawn, B. R., Role of interfacial grain-bridging sliding friction in the crack-resistance and strength properties of nontransforming ceramics. *Acta Metall.*, **37** (1989) 2659–71.
10. Rödel, J., Kelly, J. & Lawn, B. R., In situ measurements of bridged crack interfaces in the SEM. *J. Am. Ceram. Soc.*, **73** (1990) 3313–18.
11. Chantikul, P., Bennison, S. J. & Lawn, B. R., Role of grain size in the strength and *R*-curve properties of alumina. *J. Am. Ceram. Soc.*, **73** (1990) 2419–27.
12. Vekinis, G., Ashby, M. F. & Beaumont, P. W. R., *R*-curve behaviour of Al₂O₃ ceramics. *Acta Metall.*, **38** (1990) 1151–62.
13. Cook, R. F., Lawn, B. R. & Fairbanks, C. J., Microstructure–strength properties in ceramics: I. Effect of crack size on toughness. *J. Am. Ceram. Soc.*, **68** (1985) 604–15.

14. Cook, R. F., Fairbanks, C. J., Lawn, B. R. & Mai, Y.-W., Crack resistance by interfacial bridging: its role in determining strength characteristics. *J. Mater. Res.*, **2** (1987) 345–56.
15. Bennison, S. J., Padture, N. P., Runyan, J. L. & Lawn, B. R., Flaw-insensitive ceramics. *Phil. Mag. Lett.*, **64** (1991) 191–5.
16. Padture, N. P., Chan, H. M., Bennison, S. J., Runyan, J. L., Rödel, J. & Lawn, B. R., Flaw Tolerant Al₂O₃-Al₂TiO₅ composites. In *Ceramic Transactions*, Vol. 19, ed. M. D. Sacks. American Ceramic Society, Columbus, OH, 1991, pp. 715–21.
17. Lawn, B. R., Padture, N. P., Braun, L. M. & Bennison, S. J., Model for toughness-curves in two-phase ceramics: I. Basic fracture mechanics. *J. Am. Ceram. Soc.*, **76** (1993) 2241–7.
18. Padture, N. P., Runyan, J. L., Bennison, S. J., Braun, L. M. & Lawn, B. R., Model for toughness-curves in two-phase Ceramics: II. Microstructural variables. *J. Am. Ceram. Soc.* **76** (1993) 2235–40.
19. Hasselman, D. P. H. & Fulrath, R. M., Proposed fracture theory of a dispersion-strengthened glass matrix. *J. Am. Ceram. Soc.*, **49** (1966) 68–72.
20. Frey, W. J. & Mackenzie, J. D., Mechanical properties of selected glass-crystal composites. *J. Mater. Sci.*, **2** (1967) 124–30.
21. Lange, F. F., Fracture energy and strength behavior of a sodium borosilicate glass-Al₂O₃ composite system. *J. Am. Ceram. Soc.*, **54** (1971) 614–20.
22. Green, D. J. & Nicholson, P. S., Fracture of brittle particulate composites. In *Fracture Mechanics of Ceramics*, Vol. 4, ed. R. C. Bradt, D. P. H. Hasselman & F. F. Lange. Plenum Press, NY, 1978, pp. 945–60.
23. Swearingen, J. C., Beauchamp, E. K. & Eagan, R. J., Fracture toughness of reinforced glasses. In *Fracture Mechanics of Ceramics*, Vol. 4, ed. R. C. Bradt, D. P. H. Hasselman & F. F. Lange. Plenum Press, NY, 1978, pp. 973–87.
24. Faber, K. T. & Evans, A. G., Crack deflection processes: II. Experiment. *Acta Metall.*, **31** (1983) 577–84.
25. Miyata, N., Ichikawa, S., Monji, H. & Jinno, H., Fracture behavior of brittle matrix, particulate composites with thermal expansion mismatch. In *Fracture Mechanics of Ceramics*, Vol. 7, ed. R. C. Bradt, A. G. Evans, D. P. H. Hasselman & F. F. Lange. Plenum Press, NY, 1986, pp. 87–102.
26. Donald, I. W., Review—methods of improving the mechanical properties of oxide glasses. *J. Mater. Sci.*, **24** (1989) 4177–208.
27. Selsing, J., Internal stresses in ceramics. *J. Am. Ceram. Soc.*, **44** (1961) 419.
28. Hecht, N. L., McCullum, D. W. & Graves, G. A., Investigation of selected silicon nitride and silicon carbide ceramics. *Ceram. Eng. Sci. Proc.*, **9** (1988) 1313–32.
29. Bansal, N. P. & Doremus, R. H., *Handbook of Glass Properties*, Academic Press, Orlando, 1986.
30. Chantikul, P., Anstis, G. R., Lawn, B. R. & Marshall, D. B., A critical evaluation of indentation techniques for measuring fracture toughness: II. Strength method. *J. Am. Ceram. Soc.*, **64** (1981) 539–43.
31. Anstis, G. R., Chantikul, P., Marshall, D. B. & Lawn, B. R., A critical evaluation of indentation techniques for measuring fracture toughness: I. Direct crack measurements. *J. Am. Ceram. Soc.*, **64** (1981) 533–8.
32. Wiederhorn, S. M., Fracture surface energy of glass. *J. Am. Ceram. Soc.*, **52** (1969) 99–105.
33. Langitan, F. B. & Lawn, B. R., Effect of a reactive environment on the Hertzian strength of brittle solids. *J. Appl. Phys.*, **41** (1970) 3357–65.
34. Braun, L. M., Bennison, S. J. & Lawn, B. R., Objective evaluation of short-crack toughness-curves using indentation flaws: case study on alumina-based ceramics. *J. Am. Ceram. Soc.*, **75** (1992) 3049–57.
35. Frank, F. C. & Lawn, B. R., On the theory of Hertzian fracture. *Proc. Royal Soc. London*, **A299** (1967) 291–306.
36. Lawn, B. R. & Wilshaw, T. R., Indentation fracture: principles and applications. *J. Mater. Sci.*, **10** (1975) 1049–81.
37. Lawn, B. R., *Fracture of Brittle Solids*. Cambridge University Press, Cambridge, 1993.
38. Cho, S.-J., Hockey, B. J., Lawn, B. R. & Bennison, S. J., Grain-size and *R*-curve effects in the abrasive wear of alumina. *J. Am. Ceram. Soc.*, **72** (1989) 1249–52.
39. Braun, L. M., Bennison, S. J. & Lawn, B. R., Short-crack *T*-curves and damage tolerance in alumina-based composites. *Ceram. Eng. Sci. Proc.*, **13** (1992) 156–63.
40. Mai, Y.-W. & Lawn, B. R., Crack stability and toughness characteristics in brittle materials. *Ann. Rev. Mater. Sci.*, **16** (1986) 415–39.
41. Marshall, D. B., Lawn, B. R. & Chantikul, P., Residual stress effects in sharp-contact cracking: II. Strength degradation. *J. Mater. Sci.*, **14** (1979) 2225–35.
42. Lawn, B. R., Evans, A. G. & Marshall, D. B., Elastic/plastic indentation damage in ceramics: the median/radial crack system. *J. Am. Ceram. Soc.*, **63** (1980) 574–81.
43. Guiberteau, F., Padture, N. P., Cai, H. & Lawn, B. R., Indentation fatigue: a simple cyclic Hertzian test for measuring damage accumulation in polycrystalline ceramics. *Phil. Mag. A*, **68** (1993) 1003–16.
44. Runyan, J. L. & Bennison, S. J., Fabrication of flaw-tolerant aluminium-titanate-reinforced alumina. *J. Eur. Ceram. Soc.*, **7** (1991) 93–9.